Astronomy
&
Astrophysics

Calibration of the pre-main sequence RS Chamaleontis binary system

E. Alecian[1], M.-J. Goupil[1], Y. Lebreton[2], M.-A. Dupret[1], and C. Catala[1]

[1] Observatoire de Paris, LESIA, 5 place Jules Janssen, 92195 Meudon Principal Cedex, France
 e-mail: evelyne.alecian@obspm.fr
[2] Observatoire de Paris, GEPI, 5 place Jules Janssen, 92195 Meudon Principal Cedex, France

ABSTRACT

Context. The calibration of binary systems with accurately known masses and/or radii provides powerful tools to test stellar structure and evolution theory and to determine the age and helium content of stars. We study the eclipsing double-lined spectroscopic binary system RS Cha, for which we have accurate observations of the parameters of both stars (masses, radii, luminosities, effective temperatures and metallicity).
Aims. We have calculated several sets of stellar models for the components of the RS Cha system, with the aim of reproducing simultaneously the available observational constraints and to estimate the age and initial helium abundance of the system.
Methods. Using the CESAM stellar evolution code, we model both components starting from the initial mass and metallicity and adjusting the input parameters and physics in order to satisfy the observational constraints.
Results. We find that the observations cannot be reproduced if we assume that the abundance ratios are solar but they are satisfied if carbon and nitrogen are depleted in the RS Cha system with respect to the Sun. This is in accordance with the abundances observed in other young stars. The RS Cha system is in an evolutionary stage at the end of the PMS phase where models are not strongly sensitive to various physical uncertainties. However we show that the oscillations of these two stars, which have been detected, would be able to discriminate between different options in the physical description of this evolutionary phase.

Key words. stars: pre-main sequence – stars: binaries: eclipsing – stars: oscillations stars: evolution – stars: interiors – stars: individual: RS chamaleons

1. Introduction

Stellar calibration, i.e. determining masses, radii, ages of stars using theoretical stellar evolutionary tracks is a powerful tool. However, its results strongly depend upon the validity of the adopted stellar models. The physical description of these models can be validated with a small set of stars whose masses, radii, luminosities, effective temperatures and metallicities are accurately known. An eclipsing binary system is therefore an excellent candidate for such a test as the orbital information provides masses and radii and the assumed common origin of both components (implying same age and chemical composition) brings additional severe constraints to the modelling. Validation of main sequence (MS) stellar evolution models has been quite extensively performed (e.g. Noels et al. 1991; Morel et al. 2000). On the other hand, only a few validation works have so far concerned the pre-main sequence (PMS) phase. Palla & Stahler (2001) tested their PMS theoretical evolutionary tracks using eight binary systems, assuming a solar metallicity in all of them, although this assumption appeared later not to be valid in all but one case. Marques et al. (2004) modelled the binary system EK Cep using a χ^2-minimisation and obtained the most reliable set of theoretical stellar parameters that reproduces the observational ones. These authors succeeded in modelling the PMS secondary component but failed to obtain a theoretical radius that reproduces the observed one for the MS primary component.

The A-type system RS Chamaeleontis (RS Cha) is an eclipsing double-lined spectroscopic binary system. Mamajek et al. (1999) reported X-ray emission from the η Cha cluster, which indicates the PMS status of both components of RS Cha. Up to recently, all fundamental parameters of the components of this system were known, except the metallicity. However, the knowledge of the metallicity is crucial to model the structure and the evolution of these PMS stars (see Sect. 4.3.2). The metallicity of the RS Cha system that is used here has been obtained with spectroscopic data collected at the SAAO (South African Astronomical Observatory) (Alecian et al. 2005; hereafter Paper I). We took advantage of these data to redetermine the masses and radii of both stars. The resulting physical parameters of both components are detailed in Table 1.

We are then able to model these two stars and to compare the results with observations. This paper presents an advanced study of the modelling of the pre-main sequence RS Cha system. The next section describes the physical input of our standard evolution models. Section 3 states the observational constraints that our RS Cha models must reproduce. As our standard models cannot reproduce the whole set of observations, Sect. 4 investigates the sensitivity of PMS models to uncertainties in the input physics and physical parameters. Section 5 presents the final calibrated models for the RS Cha system which reproduces all the available observations. Section 6 contains an analysis of the recently discovered pulsations in both components of RS Cha and

Table 1. Fundamental parameters of RS Cha. R00: Ribas et al. (2000), CN80: Clausen & Nordström (1980), M00: Mamajek et al. (2000). P stands for primary and S for secondary.

	P	S	References
$M/M_\odot$	1.89 ± 0.01	1.87 ± 0.01	Paper I
$R/R_\odot$	2.15 ± 0.06	2.36 ± 0.06	Paper I
$T_{\rm eff}$ (K)	7638 ± 76	7228 ± 72	R00
$\log(L/L_\odot)$	1.15 ± 0.09	1.13 ± 0.09	$L = 4\pi R^2 \sigma T_{\rm eff}^4$
$\log(g)({\rm cm\,s}^{-2})$	4.05 ± 0.06	3.96 ± 0.06	$g = MG/R^2$
$v \sin i$ (km s^{-1})	64 ± 6	70 ± 6	Paper I
P (day)		1.67	Paper I
i (°)		83.4 ± 0.3	CN80
[Fe/H]		0.17 ± 0.01	Paper I

Fig. 1. Evolutionary tracks for 1.6–2.2 $M_\odot$ standard models in a HR diagram. Crosses represent observational error bars in effective temperature and luminosity (Table 1) for the primary (P) component (*left*) and for the secondary (S) component (*right*) of RS Cha. Dots indicate the onset of the radiative core, diamonds signal the convective envelope disappearance and triangles mark the convective core apparition.

discusses theoretical oscillation modes and periods. Conclusions are presented in Sect. 7.

2. Stellar modelling

We consider both stars as isolated since the system is detached. Unless it is specified, the temporal evolution of the internal structure of both stars is carried out at constant mass; hence the initial mass is set equal to the observed one. Diffusion is negligible over the duration of a PMS phase, hence we assume that the observed surface abundances correspond to the initial chemical composition. We stop the evolution when the calculated effective temperatures and luminosities correspond to the observed ones within their error bars. In the case of a binary system, the age of both components must be the same.

Our evolutionary models are computed with the CESAM code (Morel 1997); they are standard in the sense that no effect of magnetic field is included. Effects of rotation and diffusion are not included as the time scale of these phenomena are very long compared with the time spent by a star on its PMS (20 Myr for a 2 $M_\odot$).

We used the OPAL equation of state (Rogers et al. 1996) and OPAL opacities (Iglesias & Rogers 1996) complemented by Alexander & Ferguson (1994) opacities at low temperatures.

During its PMS phase, a star can possess either a convective envelope or a convective core or both. The temperature gradient in convection zones is computed using the classical mixing-length theory. The mixing length is defined as $l = \alpha H_{\rm P}$, α being the mixing length parameter and $H_{\rm P}$ the local pressure scale height, $H_{\rm P} = -\frac{{\rm d}r}{{\rm d}\ln P}$. We set the α value equal to 1.62 as obtained for a calibrated solar model calculated with the same input physics. We define the overshooting $d_{\rm ov}$ as the length of penetration of the convective eddies into the adjacent radiative zone: $d_{\rm ov} = \alpha_{\rm ov} H_{\rm P}$ with $\alpha_{\rm ov}$ the overshooting parameter. Unless otherwise specified, our models are computed without overshooting, i.e. $d_{\rm ov} = 0$.

The species entering the nuclear network are: ^{1}H, ^{3}He, ^{4}He, ^{12}C, ^{13}C, ^{14}N, ^{15}N, ^{16}O, ^{17}O. We considered ^{2}H, ^{7}Li and ^{7}Be in equilibrium and only the most important reactions of PP+CNO cycles are taken into account. The nuclear reaction rates are taken from the NACRE compilation (Angulo et al. 1999).

The metallicity, defined as [Fe/H] $= \log\left(\frac{Z/X}{(Z/X)_\odot}\right)$ where Z, X are the metal and hydrogen mass fractions respectively, is an observational constraint. Its initial value is taken equal to the observed one (Table 1) and the abundance ratios are the solar ones (Grevesse & Noels 1993). We take the initial helium mass fraction equal to the value from the solar calibration: $Y_0 = Y_\odot = 0.267$, and the hydrogen mass fraction is given
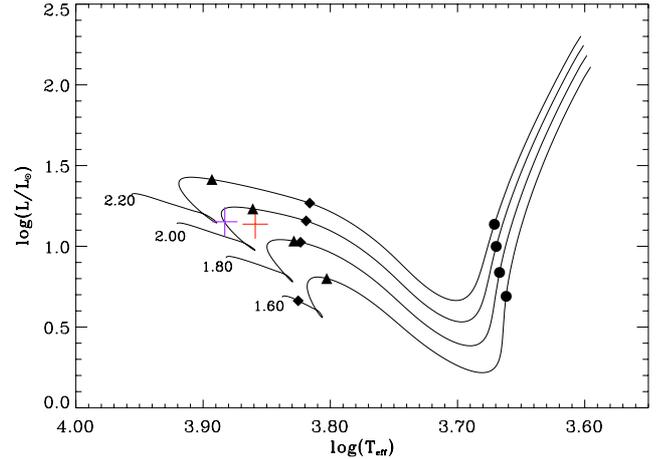
by $X_0 = \frac{1-Y_0}{1+(Z/X)_0}$. The atmosphere is calculated assuming the Eddington grey law.

Each evolution is initialized with a homogeneous, fully convective model in quasi-static contraction and we define the age of a star as the time elapsed since initialisation. Although our initial models are not realistic, recent studies have compared the evolutionary tracks during the PMS phase, considering two different initial conditions: the first model being calculated from the initial cloud contraction and the second one being calculated only from the Hayashi track (Cariulo et al. 2004, F. Palla, private communication). No fundamental differences between the two models were found and ages calculated in both cases are almost identical. So the initial conditions for the formation of the PMS star do not interfere in our study.

These stellar models will be considered from now on as our standard models.

Figure 1 shows PMS evolutionary tracks from the Hayashi line to the ZAMS for masses in the range of interest for RS Cha. We have indicated by diamonds the locus where the star becomes totally radiative and by triangles the locus where a convective core appears in the center of the star. At the stage where RS Cha is encountered, a star, evolving from the Hayashi line towards the ZAMS, has developed a fully radiative envelope and a small convective core. The earliest nuclear reactions of the CNO cycle and the p-p chain begin. The energy released by the $C^{12}(p,\gamma)N^{13}(\beta^+,\nu)C^{13}(p,\gamma)N^{14}$ chain overheats the internal regions of the star. The energy excess builds an excess pressure gradient which slows down the contraction rate in the center. At the same time, the overheating leads to the apparition of a convective core. The central regions begin to expand. The luminosity then decreases because not only do these expanding internal shells not contribute any more to the energy flux, but they blanket the nuclear source, by absorbing a large fraction of the nuclear energy produced (see detailed description of the PMS evolution in Iben 1965). For later discussions, it is important to note that the primary, as it is slightly more massive, is in a more advanced stage of evolution than the secondary. As a result, its luminosity has already decreased, unlike that of the secondary (Fig. 2).
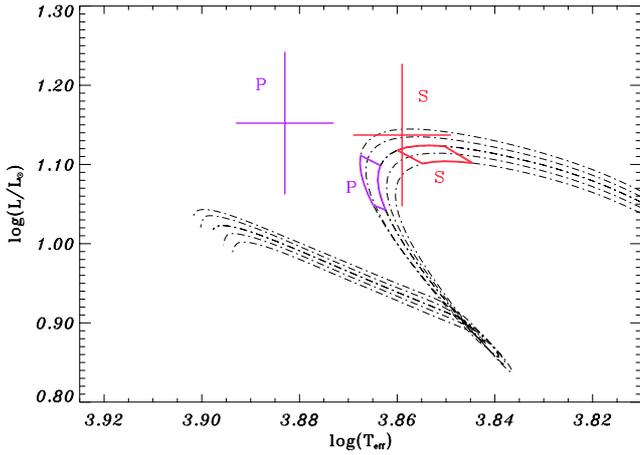
Fig. 2. Evolutionary tracks of standard models (dash-dotted lines) and error boxes in masses and radii for the primary (P) and the secondary (S) components. Crosses represent observational error bars in effective temperature and luminosity (Table 1) for the primary (P) component (*left*) and for the secondary (S) component (*right*) of RS Cha. Lowest to upper tracks are for 1.86, 1.87, 1.88, 1.89 and 1.90 $M_\odot$.

3. Observational contraints in a HR diagram

Table 1 details the physical parameters of both components of RS Cha derived from observations. Effective temperatures and luminosities as well as masses and radii will then be compared to the corresponding calculated parameters obtained using standard models. We have calculated evolutionary tracks for the observed masses of both components as well as for their extreme values given by the error bars. Figure 2 shows the end of the PMS phase of these tracks for 1.86, 1.87, 1.88, 1.89 and 1.90 $M_\odot$ masses.

For a given mass M_{obs}, a stellar model is evolved until its radius matches the observed radius R_{obs}. This provides the theoretical luminosity and effective temperature $(L, T_{eff})_{calc}$ of the model. The same is done for the extreme values of the observed masses and radii and this gives rise to error boxes which are superimposed onto the tracks in Fig. 2 as full lines. In the same graph, crosses represent the error bars in luminosity and effective temperature for the primary (left) and secondary (right) components derived from observations $(L, T_{eff})_{obs}$.

When both crosses are located inside their respective error boxes, the corresponding stellar models reproduce the observations. As can be seen in Fig. 2, this does not occur when standard models, built as detailed in the previous section, are used. Moreover, the calculated ratio of the primary to the secondary luminosities, $(L_P/L_S)_{calc}$, is lower than one, contrary to the observations, $(L_P/L_S)_{obs} = 1.05$ (Table 1). Our standard models indeed indicate that the luminosity of the P component has begun to decrease, unlike the luminosity of the S component. This implies that the P component started nuclear burning earlier than the S component (see Sect. 2).

In order for the numerical models and the observations to agree, in particular to invert the $(L_P/L_S)_{calc}$ ratio, the error box of the primary should be shifted towards greater luminosities than the secondary box. According to the evolutionary phase of the primary as described in the previous section, this means that it is necessary to delay the onset of the CNO cycle for the primary.

The way this can be achieved is discussed in the next section where we investigate the sensitivity of the stellar models in this evolutionary phase to various parameters and physical inputs.

4. Sensitivity to physical inputs and parameters

4.1. Unchanged error boxes in a HR diagram

Some physical inputs and parameters of stellar model have no effect on the location of the error boxes of RS Cha in a HR diagram:

4.1.1. Mixing length and overshoot parameters

An increase in the mixing length parameter α moves a PMS evolutionary track towards greater effective temperature and towards slightly higher luminosities, when the star possesses a convective envelope (see Böhm-Vitense 1992). But, as seen in Fig. 1, the RS Cha stars no longer have a convective envelope and changing α therefore has no effect on the error boxes.

The convective core appearing in both components is too small (less than one tenth of a stellar radius) to involve a modification of the tracks when changing the overshoot parameter α_{ov} from 0 to 0.2.

Note also that switching from a model atmosphere built assuming an Eddington grey law or based on Kurucz model atmospheres (Kurucz 1979, 1992, 1993) has no effect as the envelopes of both RS Cha components are fully radiative.

4.1.2. Equation of state

Coulomb effects and departure from a perfect gas are very small for a 2 $M_\odot$ star. Hence no variation of the tracks, whatever the evolutionary stage, is observed when using either the equation of state EFF (Eggleton et al. 1973) or the equation of state OPAL (Rogers et al. 1996).

4.1.3. Burning of light species

The light species ^2H, ^7Li and ^7Be burn at the beginning of the PMS phase during the first million years of the star, during which the gravitational energy is dominant. The energy released by the burning of light species is too small to perturb the subsequent evolutionary tracks.

4.1.4. Mass loss

PMS stars of intermediate mass are known to possess stellar winds with a mass loss rate in the range $10^{-8} - 10^{-7}$ $M_\odot$ yr^{-1} (e.g. Bouret & Catala 1998). They can also accrete mass from a surrounding disk with mass accretion rates similar to those of the wind.

We have computed PMS evolutionary tracks assuming mass loss or accretion with a rate of 10^{-8} $M_\odot$ yr^{-1}. Initial masses have been chosen such that masses of the models at the age of RS Cha (t_{RSCha}) are equal to the observed masses of RS Cha. As a consequence, although the evolutionary tracks differ before and after the age of RS Cha depending on the assumed mass loss or accretion, the error boxes of RS Cha are unaffected.

4.2. Unchanged luminosity ratio

We now discuss the physical parameters that affect the position of the error boxes in the HR diagramme but do not allow to solve the problem of the luminosity ratio. For visibility, we have removed the evolutionary tracks from the figures. Only error boxes obtained from two different models along with crosses are kept
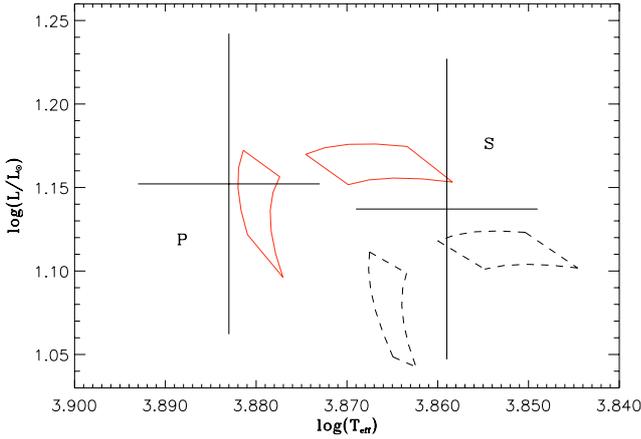
Fig. 3. Error boxes calculated by decreasing OPAL opacity of 10% (full line) and standard OPAL opacity (dashed lines). Crosses represent observational error bars in effective temperature and luminosity (Table 1) for the primary (P) component (*left*) and for the secondary (S) component (*right*) of RS Cha.

in the HR diagram. Boxes represented by dashed lines are calculated using standard models as defined in Sect. 2.1.

4.2.1. Opacity

We change the opacity (κ) in the star by diminishing it by 10%. Figure 3 shows that the error boxes are shifted towards greater luminosities and temperatures. A decrease in opacity makes the energy release easier and in order to maintain the pressure balance, models become more centrally concentrated and hotter which leads to an increase in luminosity and effective temperature (Eddington 1926). However both boxes move together towards greater temperatures and luminosities leaving the ratio L_P/L_S unchanged.

4.2.2. Helium mass fraction and metallicity

In Paper I, we determined the metallicity [Fe/H] of RS Cha (Table 1), assuming that both stars have the same chemical composition and that the metal abundance ratios are the solar ones. The knowledge of [Fe/H] gives us a constraint on Z/X for RS Cha. In order to know fully the composition of the star, we have to assume the helium mass fraction Y which is unknown for this system.

We have varied Y between the solar value: $Y = 0.267$ and $Y = 0.300$ which is a reasonable range compared to the observed values in various stars and clusters. Figure 4 shows that the luminosity and the effective temperature increase with increasing Y. An increase of Y leads to an increase of the mean molecular weight μ. In order to maintain the pressure balance the star is more condensed and hotter, which results in an increase in luminosity and effective temperature (Iben 1965).

We have also varied the metallicity of the system [Fe/H] within the error bars. Since heavy elements contribute only a small mass fraction, an increase in heavy element abundances does not influence the mean molecular weight μ very much. However an increase in metallicity increases the global opacity (κ). As seen in the previous section, an opacity increase in the whole star leads to a decrease in effective temperature and luminosity in both stars.
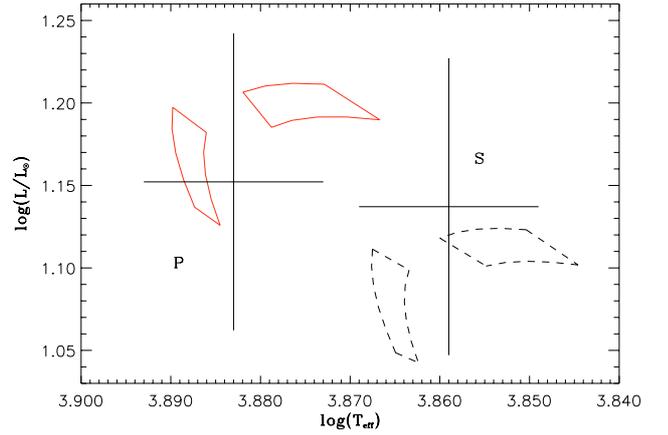

Fig. 4. Error boxes calculated by increasing the helium mass fraction while keeping Z/X constant: $Y = 0.267$ (dashed line) and $Y = 0.300$ (full line).
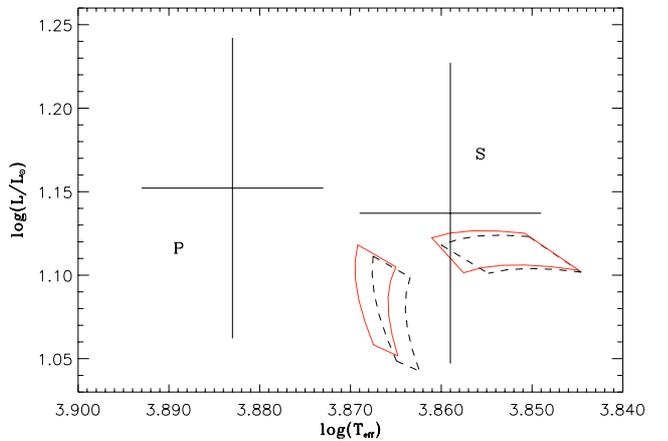

Fig. 5. Error boxes calculated by decreasing the rate of the ^{12}C(p, γ)^{13}N(e$^+$, ν)^{13}C reaction of 10% (full line) from the NACRE rate (dashed line).

As both boxes move together in the same direction, we cannot reverse the luminosity ratio by varying the helium mass fraction or the metallicity.

4.3. Inverting the luminosity ratio

So far no parameter directly or indirectly changes the luminosity transfer into the star succeeded in inverting the calculated luminosity ratio of the first component to the second one. We now focus on the energy generation.

The evolutionary stage of RS Cha corresponds to the beginning of the CNO cycle with the burning of carbon and nitrogen. The ^{12}C→^{14}N chain overheats the internal regions of the star leading to a convective core responsible for the luminosity decrease. The onset of the convective core for the primary must be delayed in order to invert the luminosity ratio; this means a decrease in the efficiency of overheating of the internal regions. This efficiency depends on both nuclear reaction rates and the abundances of the species involved in the CNO cycle.

4.3.1. Nuclear reaction rates

We first decrease the nuclear reaction rates by 10%, which corresponds to their estimated accuracy (Angulo et al. 1999). Figure 5
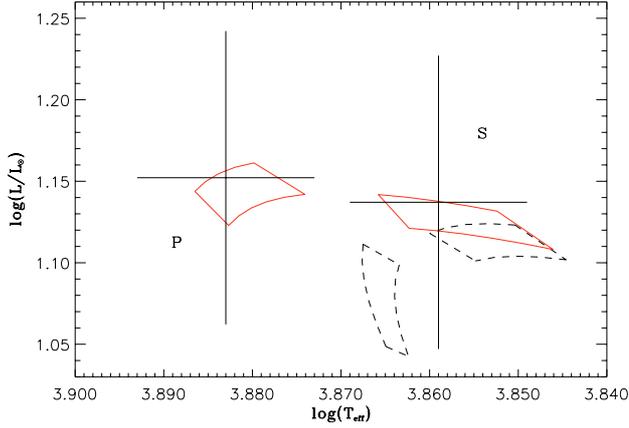
Fig. 6. Error boxes calculated by decreasing the abundance of carbon: $\Delta n_C = -0.7$ dex (full line), keeping the metallicity constant.

shows the shift of the boxes resulting from the decrease of the rate of the $^{12}C(p, \gamma)^{13}N(e^+, \nu)^{13}C$ reaction. The luminosity of the primary comes closer to that of the secondary, but not sufficiently to invert the luminosity ratio. The decrease of the rates of the other reactions of the chain $^{13}C(p, \gamma)^{14}N$ shows a similar, although smaller, shift.

4.3.2. Abundances of carbon, nitrogen and oxygen

We then decrease the abundance of carbon, nitrogen and oxygen, changing only the abundance ratios of heavy elements while keeping the metallicity unchanged. At the evolutionary stage of RS Cha the variation of the abundance of ^{17}O is very weak, compared to those of C and N, and the abundance of ^{16}O does not vary. The reason is the low rate of the reactions $^{16}O(p, \gamma)^{17}F(\beta^+, \nu)^{17}O$ and $^{17}O(p, \alpha)^{14}N$ (NACRE, Angulo et al. 1999). Hence we do not consider the oxygen abundance any further.

Hereafter we call n_i the logarithm of the abundance by number N_i of a chemical element i in a scale where the abundance of hydrogen by number is $N_H = 10^{12}$, that is

$$n_i = \log \frac{N_i}{N_H} + 12. \tag{1}$$

Figure 6 shows the shift of the error boxes resulting from a decrease of the carbon abundance n_C by 0.7 dex. As we remove some carbon, the reactions $^{12}C \rightarrow ^{13}C$ and $^{13}C \rightarrow ^{14}N$ become less efficient. The nuclear energy released ϵ is proportional to L/m, L and m being the local luminosity and mass; the radiative gradient ∇_{rad} is proportional to $\frac{L}{m}\frac{\kappa P}{T^4}$, where κ, P and T are the local opacity, pressure and temperature (e.g. Kippenhahn & Weigert 1990). We find that decreasing the abundance of carbon leads to a negligible increase of κ, P and T in the center of the star, compared to the large decrease of the L/m ratio. Therefore, by reducing the carbon abundance, the decrease of the produced nuclear energy leads to a dominant decrease of the L/m ratio, and therefore to a decrease of the radiative gradient ∇_{rad} which delays the onset of the convective core. Figure 7 shows the variation with time of the radius of each star in model 1 (normal carbon abundance) and model 2 (n_c depleted by 0.7 dex). While at ages lower than $\sim$9 Myr, the radii of the models as well as the limit between the radiative core and the convective envelope are the same, at ages higher than $\sim$9 Myr -after the onset of the CNO cycle- the convective core appears later and remains smaller in model 2.

As a result, the expansion of the internal shells is delayed, as is the decrease in total luminosity (see Sect. 2). The evolutionary track is extended towards greater luminosities and temperatures and we therefore obtain a luminosity ratio ($\frac{L_P}{L_S}$) greater than one, as observed. We notice the same phenomena with the decrease of the nitrogen abundance, which makes the reactions $^{14}N(p, \gamma)^{15}O(\beta^+, \nu)^{15}N$ and $^{15}N(p, \gamma)^{16}O$ less efficient.

5. Calibration of RS Cha

We found that the luminosity ratio $\frac{L_P}{L_S}$ is sensitive to the abundances of carbon and nitrogen. We now search for a model properly matching the observations. This model is not very different from our standard model. We must change only the abundance ratios of heavy species and the helium mass fraction. Our final models are obtained by decreasing the carbon and nitrogen abundances by 0.6 and 0.5 dex respectively. The decrease of 0.6 dex and 0.5 dex of the number of atoms of carbon and nitrogen gives new abundances equal to 8.25 and 7.77, respectively (the solar values are 8.55 and 7.97). Daflon et al. (2004) measured the abundances of various species in 69 young OB stars in 25 clusters. They found abundances between 8.21 and 8.49 for carbon and between 7.19 and 7.83 for nitrogen, showing that our values agree well with abundances observed in young stars. Our results are in the same direction as the recent solar abundances determination of Asplund et al. (2004, 2005a,b). They found a decrease of 0.16 dex in the carbon abundance and of 0.11 dex in the nitrogen abundance and of 0.21 dex in the oxygen abundance, compared to the abundances of Grevesse & Noels (1993) used in the CESAM code.

Having the appropriate luminosity ratio between both components of the system, we need to increase the helium mass fraction in order to match the calculated parameters of RS Cha to the observed ones (Table 1). The error bars in masses and radius of the models are plotted in Fig. 8. We find a value of $Y = 0.272$ ($\log(N_{He}/N_H) + 12 = 10.99$), reasonable compared to the helium mass fraction observed in young stars (Mathys et al. 2002).

Finally, it remains to be checked that both stars have the same age. We find that a common interval of ages does indeed exist inside the error boxes indicating that our final models for both components can have the same age. We illustrate this by plotting the 9.50 Myr isochrone crossing both boxes in Fig. 8. This age is of the same order as previous determinations (Mamajek et al. 2000; Luhman & Steeghs 2004). However our age determination is based on an observed metallicity unlike previous works.

In a binary system the ratio of the effective temperatures is better constrained than the absolute values of the temperatures of the individual stars. Clausen & Nordström (1980) measured very accurately the photometric value of this ratio: $T_P/T_S = 1.055 \pm 0.004$. In order to take into account this additionnal constraint, we checked that our calibration model can simultaneously reproduce this ratio and the observed radii of both stars, by plotting error boxes in the radius versus T_P/T_S diagram as follows. We first calculated the effective temperatures ranges delimited by the error boxes in masses and radii of Fig. 8 for the primary and secondary components on the same isochrone. Then we restricted these intervals to the primary and secondary temperatures which satisfy the observed ratio of T_P/T_S within the error bars. Finally we calculated by linear interpolation the corresponding radii ranges. We obtain two boxes as shown in the lower right panel of Fig. 8. We find that our calibration models reproduce the observed radii of both stars as well as the observed effective temperature ratio of the system.
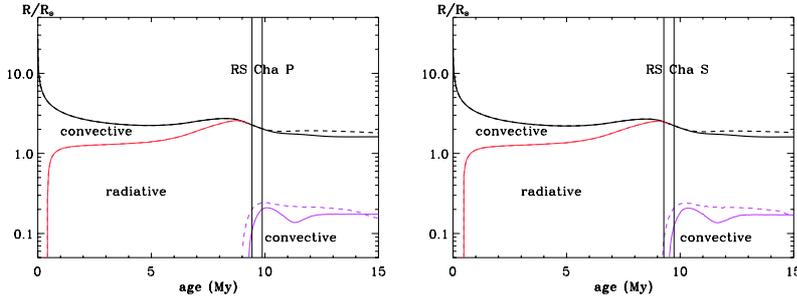
Fig. 7. Radius of the primary (*left*) and secondary (right) star plotted as a function of the age of the standard model 1 in thick-dashed-line, and model 2 built with a decrease of 0.7 dex of carbon in thick-full-line. Before ~10 Myr both radii are superimposed. The thin lines represent the limit between radiative and convective zones in model 1 (thin-dashed-line) and in model 2 (thin-full-line). The two vertical full lines represent the extrema of the age of the primary and secondary components of RS Cha (RS Cha P and RS Cha S) calculated from the error boxes P and S of Fig. 6. We see that the convective core in the secondary component is less developped than that of the primary one.
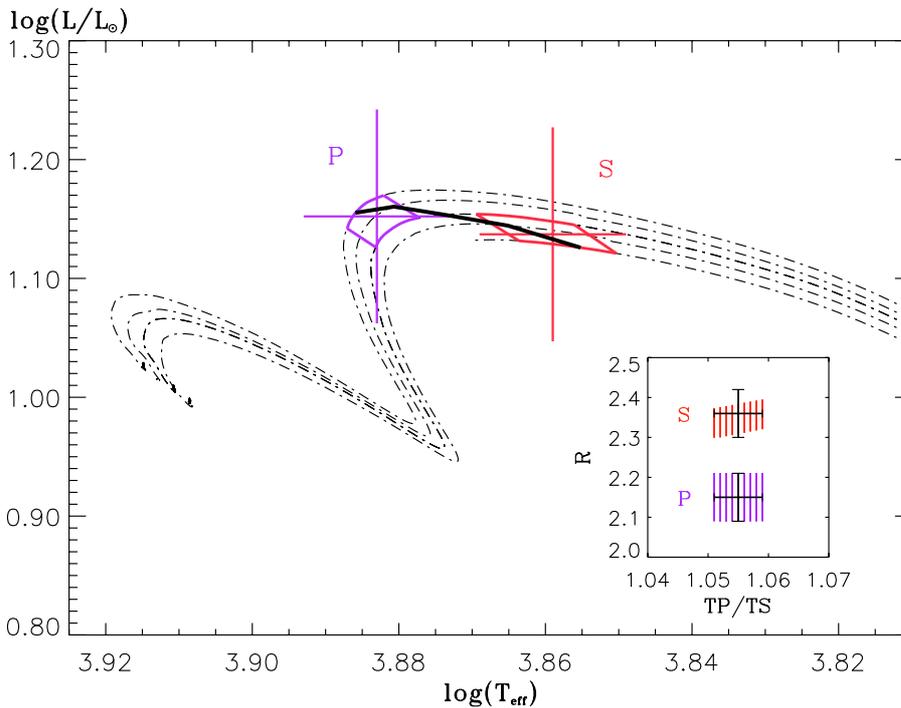

Fig. 8. Evolutionary tracks (dash-dotted lines) and error boxes (full lines) calculated by decreasing the abundances of carbon and nitrogen: $\Delta n_C = -0.6$ dex and $\Delta n_N = -0.5$ dex. The thick line is the 9.50 Myr isochrone. Crosses represent observational error bars in effective temperature and luminosity (Table 1) for the primary (P) component (*left*) and for the secondary (S) component (*right*) of RS Cha. The lower right panel shows the constraints on the radii of both stars when the photospheric measure of the effective temperature ratio of Clausen & Nordström (1980) is taken into account. Crosses represent the error bars in radii and temperature ratio for both stars. Each line in the hatched area represents the allowed values of R for a given value of T_P/T_S.

We have seen that the small area of the PMS tracks where RS Cha is observed is only weakly sensitive to various physical inputs and corresponding stellar models are then only weakly constrained. Fortunately more severe constraints can be obtained by a seismic sounding of the stellar interior, provided the stars oscillate.

6. RS Cha: a binary system of pulsating PMS stars

6.1. Observations of delta-scuti type pulsations

Many authors (Andersen 1975; McInally & Austin 1977; Palla & Stahler 2001) have discussed the possibility of the presence of oscillations in one of the components of RS Cha but reported no direct observations of these oscillations. Andersen (1975) mentioned hints of variability in the residuals from the observed radial velocity curve of the primary but could not be more conclusive with the data at his disposal. Marconi & Palla (1998) calculated the theoretical location of the instability strip of PMS stars in the HR diagram for radial modes. Palla & Stahler (2001) located RS Cha in the HR diagram and found that the secondary component lies inside the instability strip and ought to be a

PMS δ Scuti star. The primary component was found outside but near the left of the instability strip for the fundamental radial mode which cannot exclude that the star is pulsating in radial overtones and/or nonradial modes.

Finally, using our data, we have recently show, that both components of RS Cha are probably pulsating (Paper I). We have pointed out temporal variations in the residuals from radial velocity curves of both stars. These variations may be periodic with periods around one hour. We therefore ascribed them to δ Scuti type oscillations.

Unfortunately our data were not accurate enough and did not cover sufficient time to determine precisely the periods. However we can wonder whether the period around one hour found in our data belongs to the period range of the excited modes that can be expected theoretically.

6.2. Theoretical oscillation modes and periods

Theoretical periods of pulsation modes of both components of RS Cha were calculated using Dupret's code MAD (Dupret et al. 2005). This nonadiabatic code includes a time-dependent interaction between pulsation and turbulent convection
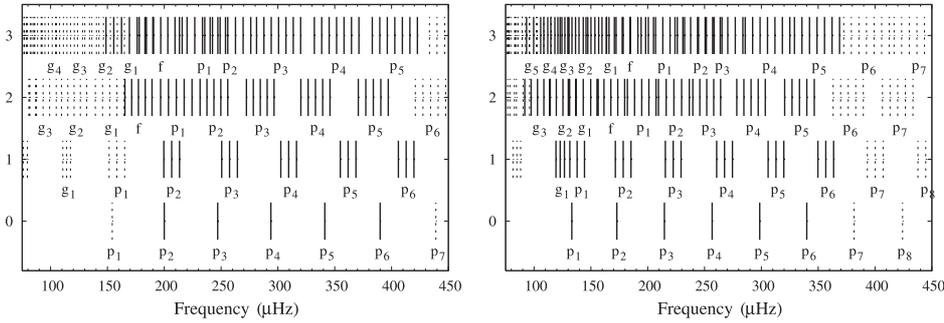
Fig. 9. Theoretical frequencies of pulsation modes obtained with non-adiabatic calculations, for the primary (*left*) and the secondary (*right*) stars. Each bar represents one mode as a function of its frequency (in μHz) and its degree ℓ (vertical direction). Dashed bars represent stable modes and solid bars unstable modes. Label p is for p mode and label g for g mode. Numbering of the label p and g referes to the radial order of the mode.

(Grigahcène et al. 2005). The blue and red edges of the instability strip are accurately determined with this code for radial and non-radial modes of MS and PMS stars (Dupret et al. 2005; Grigahcène et al. 2006).

The stellar parameters of the selected models for RS Cha components are those resulting from our calibration (see Sect. 5).

In Paper I, it was shown that the system is synchronized and the orbital period of the system has been determined accurately; we therefore know the rotational period of both stars: $P_{\rm rot} = 1.67$ d. For simplicity we assume a uniform rotation with the surface angular velocity $\Omega = 2\pi/P_{\rm rot}$. This enables us to compute the rotational splitting for each mode, according to the first order perturbation theory (Ledoux 1958)

$$\nu_{nlm} = m\Omega(1 - C_{n\ell}) \tag{2}$$

in the observer reference frame. $C_{n,\ell}$ is the Ledoux constant. These $m \neq 0$ components of the multiplets are included in the frequency set and they are assumed stable or unstable according to the same status of the associated $m = 0$ mode.

Figure 9 shows the frequency interval over which modes are unstable and therefore expected to be detected. Comparison between the plots of each component illustrates a well known result for δ Scuti like pulsations: unstable modes have higher frequencies and radial order towards the blue side of the instability strip (here the primary component).

We find that the periods of excited modes are around one hour for both stars (those of the secondary are a little longer than in the primary). On one hand, this supports the conclusion that the observed period corresponds to a low order pressure mode of delta-Scuti type and on the other hand this shows that our models are not too far from reality.

In Sect. 4.1.1., we have seen that including convective core overshoot does not change the location of the RS Cha models in the HR diagram, indicating that the structures of the models are not too affected when considering these photometric observables. We now consider the effet of including overshoot on the frequencies of each component of the system separately as an indication of the efficiency of the seismic diagnostic ability of RS Cha system.

For each component of RS Cha, we compare the frequencies for each mode $n\ell$ computed from two models which differ by the value of the overshoot parameter: one model has no overshoot $d_{\rm ov} = 0$ and the other one is computed assuming $d_{\rm ov} = 0.2H_{\rm p}$. These models selected for comparison have the

same mass and are located quite close to each other in the HR diagram. Figure 10 shows frequency differences

$$\nu_{n,\ell}^{(\rm ov)} - \nu_{n,\ell}^{(\rm noov)} \frac{\nu_{1,0}^{(\rm ov)}}{\nu_{1,0}^{(\rm noov)}} \tag{3}$$

as a function of $\nu_{n,\ell}^{(\rm noov)}$. Frequencies $\nu_{n,\ell}^{(\rm ov)}$ refer to frequencies for each oscillation mode (n, ℓ) computed from the stellar model with convective core overshoot and $\nu_{n,\ell}^{(\rm noov)}$ those for the stellar model computed assuming no convective core overshoot. The ratio $\frac{\nu_{1,0}^{(\rm ov)}}{\nu_{1,0}^{(\rm noov)}}$ is a scaling factor which corrects for the fact that the models with and without overshoot do not have the same radius.

Differences at high frequency for the secondary arise because the selected models with and without overshoot for this component have not quite the same radius and this is not completely corrected by the scaling $\nu_{1,0}^{(\rm ov)}/\nu_{1,0}^{(\rm noov)}$. On the other hand at low frequency, differences are large for the primary as the models that have been chosen for comparison have the same radius but not the same evolutionary status. Figure 10 indicates that large frequency differences arise for modes that are in the unstable range for both stars and if detected could be quite discriminant.

7. Conclusions

In this paper, we carried out a stellar modelling of a binary system whose physical parameters such as masse, radius, luminosity and effective temperature are well constrained by observations. The RS Cha system is composed of two similar intermediate mass stars in a PMS stage of evolution quite close to the ZAMS at the onset of CNO burning. Assuming that both stars have the same chemical composition, a first modelling using the spectroscopically determined iron abundance for this system and assuming solar abundance ratios could not satisfy the observational constraints simultaneously for both stars.

To obtain a consistent modelling of both stars, we investigate the sensitivity of the models in the evolutionary stage of the RS Cha system – at the end of the PMS phase – to various uncertainties in the modelling, including uncertainties in the input physics and initial abundances. We found that the stellar structure is only weakly sensitive to uncertainties in the stellar physical description.

The calibrated models i.e. the final ones that satisfy all the observational constraints were obtained only by changing the abundance ratios of carbon and nitrogen which then are in agreement with known abundances of other young stars. Once the
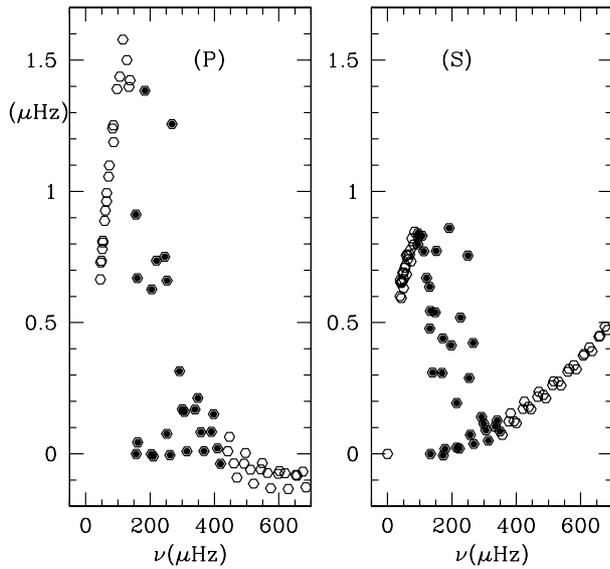
Fig. 10. Frequency differences as a function of the frequency for each oscillation mode (n, ℓ) between frequencies of one stellar model with overshoot and one without overshoot for the primary RS Cha component on the right and the secondary RS Cha component on the left. Black (resp. open) dots represent unstable (resp. stable) modes.

chemical composition is set as well as the other stellar parameters intrinsic to RS Cha stars, the error bars on the effective temperatures and luminosities, although already quite small, remain still too large to discredit the standard physical input of our stellar models. These models also satisfy the constraints on the effective temperature ratio.

We find that there is no need to include rotation in our models as they are able to reproduce the observed properties of RS Cha within their error bars. Similar conclusions are drawn by Claret (2006) in their study of EK Cep binary system. We have checked that the effects of rotation on the global parameters in the HR diagram $(L, T_{\rm eff})$ estimated from the grid of rotating atmospheres of Pérez Hernández et al. (1999) for the $v \sin i$ values of the components (Table 1) are negligible with respect to the error bars.

To obtain useful constraints on the physical description in this evolutionary phase, we therefore need to find properties of stars other than the photometric and spectroscopic ones, i.e. seismic properties. The binary system RS Cha is a good example as we have recently proved that both components are pulsating. The detected variations indicate periodicities around 1 h which we find to fall within the range of theoretically opacity driven modes with radial orders p_3-p_4 for the primary and p_4-p_5 for the secondary. We find that in this range the frequency spectra for both stars are regular when including modes with spherical degrees $\ell = 0, 2$, an advantage when dealing with mode identification and possible seismic inferences (Suran et al. 2001).

For a deeper study, however, more observations are needed in order to determine the seismic properties of both stars more precisely. This is not an easy task. This binary system is not resolved even with our largest telescopes. Therefore we cannot obtain separate photometric light curves; we can only observe the spectroscopic variations of the radial velocities of both stars. Obtaining modes and periods in this way requires long-term multi-site monotoring (which is in preparation).

References

Alecian, E., Catala, C., van't Veer-Menneret, C., Goupil, M.-J., & Balona, L. 2005, A&A, 442, 993 (Paper I)
Alexander, D. R., & Ferguson, J. W. 1994, ApJ, 437, 879
Anders, E., & Grevesse, N. 1989, Geochim. Cosmochim. Acta, 53, 197
Andersen, J. 1975, A&A, 44, 445
Angulo, C., Arnould, M., Rayet, M., et al. 1999, Nucl. Phys. A, 656, 3
Asplund, M., Grevesse, N., Sauval, A. J., Allende Prieto, C., & Blomme, R. 2005a, A&A, 431, 693
Asplund, M., Grevesse, N., Sauval, A. J., Allende Prieto, C., & Kiselman, D. 2004, A&A, 417, 751
Asplund, M., Grevesse, N., & Sauval, A. J. 2005b, in Cosmic Abundances as Records of Stellar Evolution and Nucleosynthesis, ed. T. G. Barnes, III, & F. N. Bash, ASP Conf. Ser., 336, 25
Bohm, T., & Catala, C. 1993, A&AS, 101, 629
Böhm-Vitense, E. 1992, Introduction to stellar astrophysics, Stellar structure and evolution (Cambridge, England and New York, Cambridge University Press), 3, 300
Bouret, J.-C., & Catala, C. 1998, A&A, 340, 163
Cariulo, P., Degl'Innocenti, S., & Castellani, V. 2004, A&A, 421, 1121
Claret, A. 2006, A&A, 445, 1061
Clausen, J. V., & Nordström, B. 1980, A&A, 83, 339
Cowling, T. G., & Newing, R. A. 1949, ApJ, 109, 149
Daflon, S., Cunha, K., & Butler, K. 2004, ApJ, 604, 362
Dupret, M.-A., Grigahcène, A., Garrido, R., Gabriel, M., & Scuflaire, R. 2005, A&A, 435, 927
Eddington, A. S. 1926, The Internal Constitution of the Stars (Cambridge: Cambridge University Press)
Eggleton, P. P., Faulkner, J., & Flannery, B. P. 1973, A&A, 23, 325
Grevesse, N., & Noels, A. 1993, Origin and Evolution of the Elements, ed. N. Prantzos, E. Langioni-flam, & M. Classe (Cambridge Univ. Press), 14
Grigahcène, A., Dupret, M.-A., Gabriel, M., Garrido, R., & Scuflaire, R. 2005, A&A, 434, 1055
Grigahcène, A., Dupret, M.-A., Garrido, R., Gabriel, M., & Scuflaire, R. 2006, Commun. Asteroseismol., 147, 69
Iben, I. J. 1965, ApJ, 141, 993
Iglesias, C. A., & Rogers, F. J. 1996, ApJ, 464, 943
Kippenhahn, R., & Weigert, A. 1990, Stellar Structure and Evolution, XVI, 468, 192 (Berlin Heidelberg New York: Springer-Verlag), also Astronomy and Astrophysics Library
Kurucz, R. 1993, ATLAS9 Stellar Atmosphere Programs and 2 km s^{-1} grid, (Cambridge, Mass.: Smithsonian Astrophysical Observatory)
Kurucz, R. L. 1979, ApJS, 40, 1
Kurucz, R. L. 1992, Rev. Mex. Astron. Astrofis., 23, 45
Ledoux, P. 1958, Handbuch der Physik, 51, 605
Luhman, K. L., & Steeghs, D. 2004, ApJ, 609, 917
Mamajek, E. E., Lawson, W. A., & Feigelson, E. D. 1999, ApJ, 516, L77
Mamajek, E. E., Lawson, W. A., & Feigelson, E. D. 2000, ApJ, 544, 356
Marconi, M., & Palla, F. 1998, ApJ, 507, L141
Marques, J. P., Fernandes, J., & Monteiro, M. J. P. F. G. 2004, A&A, 422, 239
Mathys, G., Andrievsky, S. M., Barbuy, B., Cunha, K., & Korotin, S. A. 2002, A&A, 387, 890
McInally, C. J., & Austin, R. D. 1977, Informational Bulletin on Variable Stars, 1334, 1
Morel, P. 1997, A&AS, 124, 597
Morel, P., Provost, J., Lebreton, Y., Thévenin, F., & Berthomieu, G. 2000, A&A, 363, 675
Noels, A., Grevesse, N., Magain, P., et al. 1991, A&A, 247, 91
Palla, F., & Stahler, S. W. 2001, ApJ, 553, 299
Pérez Hernández, F., Claret, A., Hernández, M. M., & Michel, E. 1999, A&A, 346, 586
Ribas, I., Jordi, C., Torra, J., & Giménez, Á. 2000, MNRAS, 313, 99
Rogers, F. J., Swenson, F. J., & Iglesias, C. A. 1996, ApJ, 456, 902
Suran, M., Goupil, M., Baglin, A., Lebreton, Y., & Catala, C. 2001, A&A, 372, 233